Journal of Applied Physics | ARTICLE | pubs.aip.org/aip/jap

Enhanced Q-factor in microcantilevers using stiffened inertial amplifiers

Cite as: J. Appl. Phys. **136**, 204503 (2024); doi: 10.1063/5.0237524
Submitted: 5 September 2024 · Accepted: 13 November 2024 ·
Published Online: 26 November 2024

View Online Export Citation CrossMark

Sondipon Adhikari[a)] and Sudip Chowdhury[b)]

AFFILIATIONS

James Watt School of Engineering, The University of Glasgow, Glasgow, Scotland, United Kingdom

[a)]**Electronic mail:** Sondipon.Adhikari@glasgow.ac.uk
[b)]**Author to whom correspondence should be addressed:** Sudip.Chowdhury@glasgow.ac.uk

ABSTRACT

Microcantilevers are widely employed in sensing applications because they are highly sensitive to changes in vibrational frequency. The Q-factor, a measure of the effectiveness of energy storage in resonant systems, is a crucial parameter that directly influences the sensitivity and performance of microcantilevers. Conventional approaches to improving the Q-factor by choosing certain materials or making changes to the shape have notable practical and economic constraints. This study introduces a new method that utilizes reinforced inertial amplifiers to significantly improve the Q-factor of microcantilevers. We introduce three setups: the standard amplifier, the compound amplifier, and the nested amplifier, each specifically engineered to enhance the system's effective inertia. According to theoretical modeling, all arrangements enhance the Q-factor, with the nested design resulting in an impressive amplification of over 3000. These findings present a scalable technique to improve the sensitivity of microcantilevers, offering a potential approach for future experimental verification and utilization in precision sensing technologies.

I. INTRODUCTION

Microcantilevers are extensively utilized in diverse scientific and technological domains owing to their exceptional sensitivity to alterations in vibrational frequency and bending. These small beams are crucial elements of sensors used to detect physical, chemical, and biological properties at a very small scale.[1] They are extremely important in fields such as atomic force microscopy (AFM), scanning probe microscopy (SPM), and biosensing.[2,3] The performance of these microcantilevers is commonly evaluated using the Q-factor, which is a dimensionless quantity that quantifies the efficiency of energy storage compared to the energy dissipated in each oscillation cycle.[4] A higher Q-factor indicates increased sensitivity, enhanced precision, and extended oscillation durations, all of which are crucial for numerous sensing applications.[5] Nevertheless, increasing the Q-factor in microcantilevers poses considerable difficulties, especially when depending on conventional approaches like material optimization or geometry alterations. This research tackles these difficulties by presenting a new method[6] for enhancing the Q-factor by incorporating reinforced inertial amplifiers.[7] The primary novelty of the current research is the use of three distinct amplification configurations to raise the Q-factor of microcantilevers, particularly engineered to augment effective inertia and overcome the constraints of traditional methods. Reference 6 introduces an inertial amplification method for low-frequency vibration energy harvesting; however, our research goes further on this idea by developing three distinct designs aimed at enhancing the Q-factor in microcantilever systems. This technique not only broadens the possible uses of inertial amplifiers but also offers a new strategy for systematically enhancing the Q-factor, which is not examined in Ref. 6.

Microcantilevers act as resonant structures that oscillate in reaction to external stimuli, enabling them to perceive minuscule alterations in mass,[8] force, or environmental circumstances.[9] When a particle or molecule sticks to the surface of a microcantilever, it changes the resonance frequency of the device, which gives a detectable signal that can be used to identify certain substances.[10,11] Microcantilevers are well suited for use in environmental monitoring, gas sensing, and biological detection due to their ability to provide high sensitivity and selectivity, which are crucial in these applications.[12] Atomic force microscopy uses microcantilevers that are outfitted with nanoscale tips to achieve atomic-resolution imaging of surfaces.[13,14] This is accomplished by scanning the tips across samples and quantifying the contact forces between the tip and the surface.

The sensitivity of microcantilevers in these applications is directly proportional to their Q-factor.[15] A higher Q-factor leads to decreased energy dissipation, enabling the cantilever to maintain oscillations for an extended duration, hence improving its sensitivity to detect minute alterations.[16,17] Furthermore, an increased Q-factor results in a narrower resonance bandwidth, which in turn produces more distinct resonance peaks and enhances the precision of frequency shift measurements.[18] Precision is crucial when it comes to identifying minuscule amounts of mass since even the tiniest interactions can result in noticeable shifts in frequency.[19] A high Q-factor is essential in AFM for achieving high-resolution surface imaging, and in biosensing, it facilitates the precise identification of tiny molecules like proteins or viruses.[20]

Improving the Q-factor in microcantilevers is a challenging task, despite its significant relevance.[21] The Q-factor is determined by various elements, including material characteristics, geometric configuration, and ambient circumstances.[22] In the past, researchers have tried to enhance the Q-factor by improving the materials used to make the cantilevers. This involves choosing materials with low internal friction or excellent mechanical quality.[23] An alternative method involves altering the structural design of the cantilevers, such as by modifying their thickness, length, or width, in order to reduce energy dissipation.[24] Nevertheless, these techniques are frequently limited by practical constraints, such as the accessibility of appropriate materials, the intricacy of manufacture, and cost considerations.[25]

In addition, the Q-factor can be significantly affected by external factors such as air damping, support losses, and temperature variations. This is particularly true in real-world scenarios where it is challenging to maintain optimal environmental conditions.[26] Air damping is a phenomenon that occurs when the microcantilever interacts with the surrounding medium, resulting in the dissipation of energy. Support losses, resulting from the linkage between the cantilever and its mounting, can also diminish the Q-factor.[27] Although certain losses can be reduced by working in vacuum settings or employing specific mounting techniques, these solutions are either impracticable or excessively costly for general implementation.[28] Considering these difficulties, it is necessary to develop creative methods to improve the Q-factor without exclusively depending on the material or geometric optimization.[29] It is crucial for applications that need high sensitivity, such as biosensors or AFM, as even slight enhancements in the Q-factor can result in substantial improvements in performance.[30]

This work presents a new technique for improving the Q-factor of microcantilevers by employing stiffening inertial amplifiers. Inertial amplifiers function by augmenting the effective inertia of a vibrating system, therefore diminishing energy dissipation and enhancing the Q-factor. The method we employ consists of affixing reinforced inertial amplifiers to the ends of microcantilevers, enabling enhanced manipulation of the system's dynamic reaction. We are examining three distinct configurations: the standard stiffened inertial amplifier, the compound amplifier, and the nested amplifier. Each of these designs utilizes the principles of inertial amplification to improve the performance of microcantilevers. The conventional rigidified inertial amplifier employs a solitary rhombus mechanism, including inflexible links and affixed masses, therefore, significantly augmenting the cantilever's inertia. The compound amplifier enhances the design by integrating several smaller inertial amplifiers that operate together, resulting in a greater amplification of inertia. The nested stiffened inertial amplifier is composed of interconnected mechanisms nested within each other, resulting in the most significant level of amplification. By employing theoretical modeling and analysis, we establish that all three designs notably enhance the Q-factor. The layered design, in particular, achieves an amplification factor above 3000. This study introduces a scalable and effective technique to improve the Q-factor in microcantilevers, addressing several constraints encountered by conventional methods. Utilizing stiffened inertial amplifiers offers a new method for enhancing sensitivity in sensing applications without requiring expensive alterations to materials or geometry. The ramifications of our discoveries are substantial for several applications, such as chemical and biological sensing, where enhanced sensitivity and precision are crucial. Moreover, this study establishes the groundwork for future experimental confirmation and enhancement, with the capability to revolutionize the development of microcantilever-based sensors that exhibit exceptional performance.

II. DYNAMICS OF A DAMPED CANTILEVER

Due to the small thickness-to-length ratio, the Euler–Bernoulli beam theory can be used to model the bending vibration of such microcantilevers. The equation of motion of a damped cantilever modeled using Euler–Bernoulli beam theory can be expressed as

$$EI\frac{\partial^4 w(x,t)}{\partial x^4} + c_1\frac{\partial^5 w(x,t)}{\partial x^4 \partial t} + \rho A\frac{\partial^2 w(x,t)}{\partial t^2} + c_2\frac{\partial w(x,t)}{\partial t} = F(x,t). \quad (1)$$

In the above equation, x is the coordinate along the length of the beam, t is the time, E is Young's modulus, I is the second moment of the cross-section, A is the cross-section area, ρ is the density of the material, $F(x,t)$ is the applied spatial dynamic forcing, and $w(x,t)$ is the transverse displacement. The length of the beam is assumed to be L. Additionally, c_1 is the strain-rate-dependent viscous damping coefficient, and c_2 is the velocity-dependent viscous damping coefficient. A schematic diagram of a cantilever is shown in Fig. 1(a). The boundary conditions associated with Eq. (1) can be expressed as

$$\begin{gathered} w(0,t)=0, \quad w'(0,t)=0, \\ w''(L,t)=0 \text{ and } w'''(L,t)=0. \end{gathered} \quad (2)$$

Here, $(\bullet)'$ denotes the derivative respective to x.

In the majority of applied physics and engineering applications, the first mode of vibration is considered. For this special case, without any loss of generality, an equivalent damped single degree of freedom (SDOF) model, as shown in Fig. 1(b), can be used. For a damped beam, the equivalent SDOF model can be obtained rigorously using the Galerkin approach. Alternatively, using cubic displacement functions with the boundary conditions

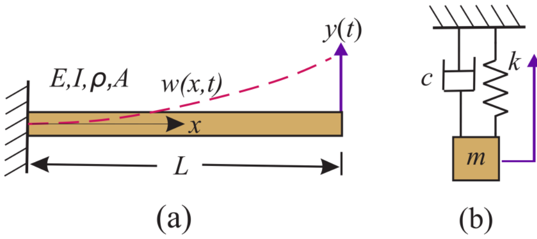

FIG. 1. Schematic diagrams of (a) A damped cantilever beam, and (b) The equivalent damped single degree of freedom (SDOF) oscillator model.

in Eq. (2), the equation of motion of free vibration of the equivalent SDOF system can be expressed as

$$m\ddot{y}(t) + c\dot{y}(t) + ky(t) = 0. \tag{3}$$

Here,

$$m = \frac{33}{140}\rho AL, \quad k = \frac{3EI}{L^3}, \quad \text{and} \quad c = \alpha k + \beta m \tag{4}$$

with $\alpha = c_1/EI$ and $\beta = c_2/\rho A$. Here, the undamped natural frequency (ω) and the damping factor (ζ) are expressed as

$$\omega_n = \sqrt{\frac{k}{m}} \tag{5}$$

and

$$\frac{c}{m} = 2\zeta\omega_n \quad \text{or} \quad \zeta = \frac{c}{2\sqrt{\text{km}}}. \tag{6}$$

The equivalent damped single degree of freedom (SDOF) model in this picture effectively depicts the essential components of our system, including the mass, stiffness, and damping elements. The strain rate-dependent damping is inherently included in the damping term of the governing equations, influencing the system's overall damping behavior. This factor affects the dynamic response, especially under situations of elevated deformation rates.

The complex natural frequencies of the system are given by

$$\lambda_{1,2} = -\zeta\omega_n \pm \mathrm{i}\omega_n\sqrt{1-\zeta^2} = -\zeta\omega \pm \mathrm{i}\omega_d. \tag{7}$$

Here, the imaginary number $\mathrm{i} = \sqrt{-1}$ and the damped natural frequency is expressed as

$$\omega_d = \omega_n\sqrt{1-\zeta^2}. \tag{8}$$

The Quality factor (Q-factor) of an oscillator is the ratio between the energy stored and energy lost during one cycle when the oscillator vibrates at the resonance frequency. It can be shown that the Q-factor

$$Q = \frac{m\omega_d}{c} = \frac{\sqrt{1-\zeta^2}}{2\zeta} \approx \frac{1}{2\zeta}. \tag{9}$$

The above approximation arises in the case of lightly damped systems. Next, we investigate how the Q-factor changes when an inertial amplifier is attached to the cantilever.

III. THE DYNAMICS OF THE CANTILEVER BEAMS WITH STIFFENED INERTIAL AMPLIFIERS

A. Stiffened inertial amplifiers

The structural diagram of the stiffened inertial amplifier is illustrated in Fig. 2, which is affixed to the point of the cantilever beam.

The inertial amplifier is constructed by placing masses m_a within a rhombus mechanism made of four rigid links. The amplifier angle is ϕ with respect to the vertical line, and it is assumed that the rhombus mechanism can move freely in a frictionless manner about the hinges marked in Fig. 2 by green dots. The displacements of the cantilever tip (at point A) and the amplifier mass (at point O) are denoted by $y(t)$ and $u(t)$, respectively. The motions $y(t)$ and $u(t)$ are perpendicular to each other. Note that due to the symmetry of the mechanism, the dynamics at points O and O' are the same. Therefore, it is sufficient to consider the dynamic equilibrium at one point only. The internal force within the rigid link bars in the upper half of the mechanism. The vertical motion of point O is derived as $y_a(t) = y(t)/2$ due to the vertical symmetry of the mechanism. Considering the bars in Fig. 2 are rigid, using the

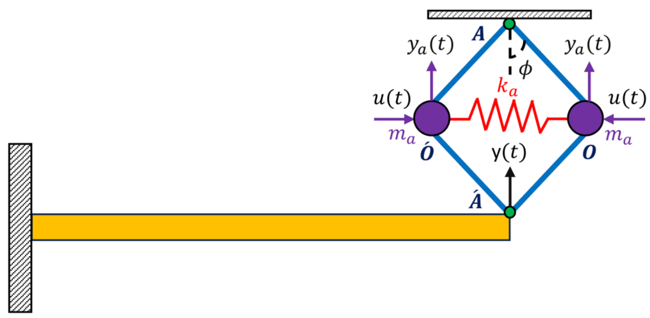

FIG. 2. A small amplitude free vibration is applied to a cantilever beam that is equipped with a stiffened inertial amplifier. The amplifier is affixed to the upper portion of the cantilever beam. The static mass, rigidity, and damping of the beam are expressed as m, k, and c, correspondingly. Two masses m_a are located at the two horizontal terminals of the inertial amplifier. The amplifier's rigidity, k_a, is determined by the spring that connects these two masses. The amplifier angle, denoted as ϕ, is the angle formed by the rhombus-type structural configuration of the inertial amplifier at its joints. $y(t)$ and $u(t)$ represent the displacement of the amplifier (at point O) and the apex of the beam (at point A'). The static mass, stiffness, and damping of the cantilever beam are increased to the effective mass, stiffness, and damping, which are m_e, k_e, and c, as a result of these deflections. The Q-factor of the cantilever beam is improved by its effective attenuation.

kinematic relationship of the rigid bars, the deflections of the inertial amplifier masses, i.e., m_a, at horizontal and vertical directions are derived as

$$\begin{aligned} \tfrac{y(t)}{2}\cos\phi = u(t)\sin\phi \quad \text{or} \quad \mathrm{u(t)} = \tfrac{\mathrm{y(t)}\cot\phi}{2}, \\ y_a(t) = \tfrac{y(t)}{2}. \end{aligned} \tag{10}$$

The velocity of the amplifier masses is derived as

$$\begin{aligned} \dot{u}(t) = \tfrac{\dot{y}(t)\cot\phi}{2}, \\ \dot{y}_a(t) = \tfrac{\dot{y}(t)}{2}. \end{aligned} \tag{11}$$

Here, $(\bullet)$ defines the derivative with respect to time. The total kinetic energy of the cantilever beam with an inertial amplifier has been derived as

$$T = \frac{1}{2}m\dot{y}^2(t) + 2\times\frac{1}{2}m_a\left(\dot{u}^2(t) + \dot{y}_a^2(t)\right). \tag{12}$$

Equation (11) has been substituted in Eq. (12). The kinetic energy is derived as

$$T = \frac{1}{2}m\dot{y}^2(t) + m_a\left(\frac{\dot{y}^2(t)\cot^2\phi}{4} + \frac{\dot{y}^2(t)}{4}\right). \tag{13}$$

The total potential energy of the cantilever beam with an inertial amplifier has been derived as

$$U = \frac{1}{2}ky^2(t) + \frac{1}{2}k_a(2u(t))^2. \tag{14}$$

The first expression of Eq. (10) has been substituted in Eq. (14). The potential energy is derived as

$$U = \frac{1}{2}ky^2(t) + \frac{1}{2}k_a y^2(t)\cot^2\phi. \tag{15}$$

The total damping energy of the cantilever beam with an inertial amplifier has been derived as

$$D = \frac{1}{2}c\dot{y}^2(t). \tag{16}$$

Lagrange's equation for free vibration is derived and expressed as

$$\frac{d}{dt}\left(\frac{\partial T}{\partial \dot{y}(t)}\right) - \frac{\partial T}{\partial y(t)} + \frac{\partial U}{\partial y(t)} + \frac{\partial D}{\partial \dot{y}(t)} = 0. \tag{17}$$

Equations (13), (15), and (16) are substituted in Eq. (17). Accordingly, the governing equation of motion has been derived as

$$\underbrace{\left(m + \frac{m_a}{2}\left(1+\cot^2\phi\right)\right)}_{me}\ddot{y}(t) + c\dot{y} + \underbrace{\left(k + k_a\cot^2\phi\right)}_{ke}y(t) = 0, \tag{18}$$

where the effective damping, i.e., c, has been derived as

$$c = 2m\zeta\omega_n, \tag{19}$$

where ζ and ω_n define the damping ratio and frequency of the cantilever beam. Equation (18) has been re-written as

$$m\left(1 + \frac{\mu_a}{2}\left(1+\cot^2\phi\right)\right)\ddot{y}(t) + c\dot{y} + k\left(1 + \kappa_a\cot^2\phi\right)y(t) = 0, \tag{20}$$

where the mass and stiffness ratios are given by

$$\mu_a = \frac{m_a}{m} \quad \text{and} \quad \kappa_a = \frac{k_a}{k}. \tag{21}$$

The non-dimensional *inertial amplification factor* as the ratio of the effective mass of the inertially amplified system to the original system as

$$\Gamma_m = \frac{m_e}{m} = 1 + \frac{\mu_a}{2}(1+\cot^2\phi). \tag{22}$$

Similarly, the non-dimensional *stiffness factor* has been derived as

$$\Gamma_k = \frac{k_e}{k} = 1 + \kappa_a\cot^2\phi. \tag{23}$$

A force $p(t)$ is applied at the beam with an inertial amplifier. Use the above parameters, the equation of motion in Eq. (20) can be expressed with the forcing term $p(t)$ as

$$m\Gamma_m\ddot{y}(t) + c\dot{y}(t) + k\Gamma_k y(t) = p(t), \tag{24}$$

where the value of c has been derived as

$$c = 2m\zeta\omega_n. \tag{25}$$

Equation (25) has been substituted in Eq. (24) and the governing equation of motion has been derived as

$$m\Gamma_m\ddot{y}(t) + 2m\zeta\omega_n\dot{y}(t) + k\Gamma_k y(t) = p(t). \tag{26}$$

Next, the Q-factor of the amplified system is quantified.

The stiffened inertial amplifier discussed in this section has the potential for enhanced effective inertia. Here, we aim to introduce two new designs that may further enhance the inertial amplification and, consequently, the Q-factor amplification.

B. The compound stiffened inertial amplifier

The main idea behind the compound inertial amplifier is to have multiple smaller inertial amplifiers working in unison. The proposed design of a compound inertial amplifier with two cells is shown in Fig. 3. Two secondary mechanisms are inserted within a primary mechanism. From a practical standpoint, the outer and inner mechanisms can be placed in offset vertical planes so that their movements do not intersect each other. The primary amplifier angle is ϕ, and the secondary amplifier angle is θ. Each mass within the cells is $m_a/2$, so the total mass in each half is m_a, as in the case of the stiffened inertial amplifier discussed in Sec. III A. This way, the inertial amplification performance can be compared consistently across different designs. Lagrange's equation in Eq. (17) has been applied to derive the governing equations of

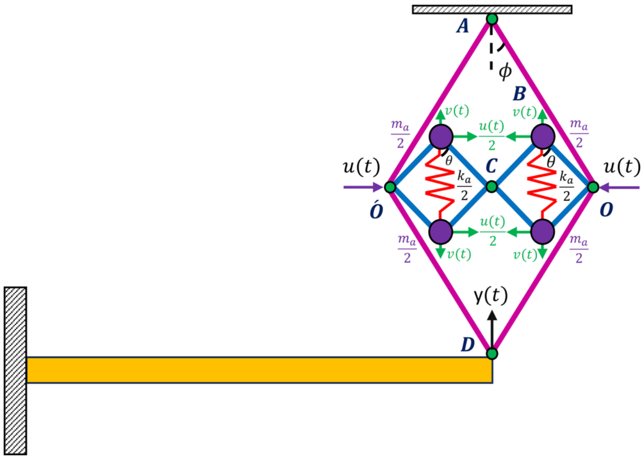

FIG. 3. A cantilever beam with compound inertial amplifier. A compound inertial amplifier with two cells. The primary amplifier angle is ϕ, and the secondary amplifier angle is θ. Each mass within the cells is $m_a/2$ so that the total mass is the same as the conventional inertial amplifier. The displacement of the mass (at point D), point O, and the amplifier mass (at point B) are denoted by $y(t)$, $u(t)$, and $v(t)$, respectively. The forces $F_1(t)$, $F_2(t)$, and $F_3(t)$ are the internal forces within the rigid links of the primary and secondary mechanisms.

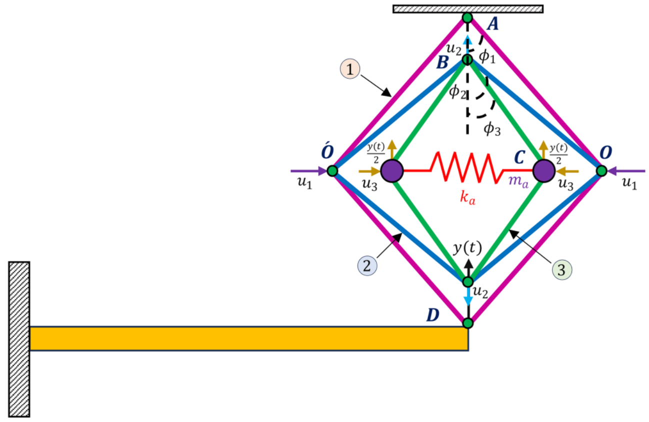

FIG. 4. A cantilever beam with the nested inertial amplifier. The nested inertial amplifier is made of three connected mechanisms. The mass m_a is placed inside the innermost mechanism. The amplifier angles for the mechanisms are ϕ_1, ϕ_2, and ϕ_3 as shown. The displacement of the mass (at point D), points O, B, and C are denoted by $y(t)$, $u_1(t)$, $u_2(t)$, and $u_3(t)$, respectively. The forces $F_i(t)$, $i = 1, \ldots, 4$ are the internal forces within the rigid links of the mechanism 1, 2, and 3, respectively.

motion of the cantilever beam with a compound stiffened inertial amplifier and expressed as

$$\underbrace{\left(m+\frac{m_a}{8}\cot^2\phi\left(1+\tan^2\theta\right)\right)}_{me}\ddot{y}(t)+c\dot{y}+\underbrace{\left(k+k_a\cot^2\phi\frac{\tan^2\theta}{4}\right)}_{ke}y(t)=0. \tag{27}$$

The non-dimensional mass and stiffness ratios are given by

$$\mu_a=\frac{m_a}{m}\quad\text{and}\quad\kappa_a=\frac{\mathrm{k_a}}{\mathrm{k}}. \tag{28}$$

The non-dimensional *inertial amplification factor* as the ratio of the effective mass of the inertially amplified system to the original system as

$$\Gamma_m=\frac{m_e}{m}=1+\frac{\mu_a}{8}\cot^2\phi\left(1+\tan^2\theta\right). \tag{29}$$

Similarly, the non-dimensional *stiffness factor* has been derived as

$$\Gamma_k=\frac{k_e}{k}=1+\kappa_a\cot^2\phi\frac{\tan^2\theta}{4}. \tag{30}$$

C. The nested stiffened inertial amplifier

In Sec. III B, we show that inertial amplification can be enhanced by introducing secondary mechanisms within the primary mechanism. Motivated by this, here we take this idea further in the form of a nested inertial amplifier design shown in Fig. 4. The amplifier is obtained by introducing two connected four-bar rhombus mechanisms inside the primary mechanism. The overall design conceived in Fig. 4 is, therefore, made of three mechanisms, and they are marked on the figure. The amplifier mass m_a is placed inside the innermost mechanism. Therefore, the amount of amplifier mass employed is the same as in the previous two cases. The outer and both inner mechanisms can be placed in offset vertical planes so that their movements do not intersect each other. Lagrange's equation in Eq. (17) has been applied to derive the governing equations of motion of the cantilever beam with a compound stiffened inertial amplifier and expressed as

$$\underbrace{\left(m+\frac{m_a}{2}\left(1+\cot^2\phi_3\right)\cot^2\phi_1\tan^2\phi_2\right)}_{me}\ddot{y}(t)$$
$$+c\dot{y}+\underbrace{\left(k+k_a\cot^2\phi_1\left(\tan^2\phi_2\cot^2\phi_3\right)\right)}_{ke}y(t)=0. \tag{31}$$

The non-dimensional mass and stiffness ratios are given by

$$\mu_a=\frac{m_a}{m}\quad\text{and}\quad\kappa_a=\frac{k_a}{k}. \tag{32}$$

The non-dimensional *inertial amplification factor* as the ratio of the effective mass of the inertially amplified system to the original system as

$$\Gamma_m=\frac{m_e}{m}=1+\frac{\mu_a}{2}\left(1+\cot^2\phi_3\right)\cot^2\phi_1\tan^2\phi_2. \tag{33}$$

Similarly, the non-dimensional *stiffness factor* has been derived as

$$\Gamma_k = \frac{k_e}{k} = 1 + \kappa_a \cot^2\phi_1\left(\tan^2\phi_2\cot^2\phi_3\right). \tag{34}$$

IV. THE QUANTIFICATION OF THE Q-FACTOR

The characteristic equation corresponding to the equation of motion Eq. (26) is given by

$$\lambda^2 m\Gamma_m + 2\lambda m\zeta\omega_n + k\Gamma_k = 0. \tag{35}$$

Diving by m, we can rewrite

$$\lambda^2\Gamma_m + 2\lambda\zeta\omega_n + \omega_n^2\Gamma_k = 0. \tag{36}$$

Solving this equation for λ, the two roots are

$$\lambda_{1,2} = \frac{\left(-\zeta \pm \sqrt{\zeta^2 - \Gamma_m\Gamma_k}\right)\omega_n}{\Gamma_m}. \tag{37}$$

The right-hand side of the above expression can be rearranged to express the complex natural frequencies of the system as

$$\lambda_{1,2} = -\zeta_a\omega_a \pm \mathrm{i}\omega_a\sqrt{1-\zeta_a^2}. \tag{38}$$

Here, the undamped natural frequency (ω_a) and the damping factor (ζ_a) of the amplified system (denoted by the subscript a) are given by

$$\omega_a = \omega_n\frac{\sqrt{\Gamma_k}}{\sqrt{\Gamma_m}} \quad \text{and} \quad \zeta_a = \frac{\zeta}{\sqrt{\Gamma_k}\sqrt{\Gamma_m}}. \tag{39}$$

From the preceding equation, the Q-factor of the amplified system can be expressed as

$$Q_a = Q\left(\sqrt{\Gamma_k}\sqrt{\Gamma_m}\right). \tag{40}$$

This is one of the key results in the paper as it quantifies the Q-factor of the inertially amplified cantilever. To understand this more clearly, we define the dimensionless *Q-factor amplification coefficient* as

$$\Gamma_Q = \frac{Q_a}{Q} = \sqrt{\Gamma_k}\sqrt{\Gamma_m}. \tag{41}$$

For the stiffened inertial amplifier shown in Fig. 2, the Q-factor amplification coefficient is, therefore, obtained as

$$\Gamma_{Q_1} = \sqrt{\left(1+\kappa_a\cot^2\phi\right)\left(1+\frac{\mu_a}{2}\left(1+\cot^2\phi\right)\right)}. \tag{42}$$

Here, subscript 1 is used to denote that the inertial amplifier in Fig. 2 is the first design introduced in the paper.

For the second design, the compound stiffened inertial amplifier shown in Fig. 3, the Q-factor amplification coefficient is therefore obtained as

$$\Gamma_{Q_2} = \sqrt{\frac{\left(1+\kappa_a\cot^2\phi\frac{\tan^2\theta}{4}\right)}{\left(1+\frac{\mu_a}{8}\cot^2\phi(1+\tan^2\theta)\right)}}. \tag{43}$$

Here, subscript 2 is used to denote that the inertial amplifier in Fig. 3 is the second design introduced in the paper.

For the third design, the nested stiffened inertial amplifier shown in Fig. 4, the Q-factor amplification coefficient is, therefore, obtained as

$$\Gamma_{Q_3} = \sqrt{\frac{\left(1+\kappa_a\cot^2\phi_1\tan^2\phi_2\cot^2\phi_3\right)}{\left(1+\frac{\mu_a}{2}\left(1+\cot^2\phi_3\right)\cot^2\phi_1\tan^2\phi_2\right)}}. \tag{44}$$

Here, subscript 3 is used to denote that the inertial amplifier in Fig. 4 is the third design introduced in the paper. In Fig. 5, the Q-factor amplification coefficient is plotted as a function of the amplifier angle ϕ. It has been observed that the Q-factor amplification increases when the amplifier angle ϕ is closer to $\phi \geq 5^\circ$. This result shows that the theoretical Q-factor amplification can be over 30. The two key assumptions made in deriving the equation of motion are (1) the hinge movements between the four-link bars, the mass, and the ground are frictionless and (2) the masses of the four-link bars are negligible. When the amplifier angle ϕ becomes close to zero, the mechanism becomes extremely narrow, and even very small friction in the hinges will prevent it from operating properly. Keeping this in mind, it is preferable that $\phi \geq 10^\circ$. This will ensure that the assumptions made apply to our model.

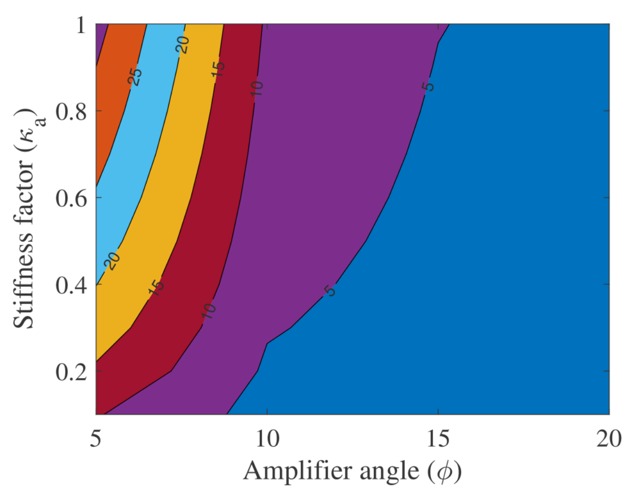

FIG. 5. The contour graph of the Q-factor amplification coefficient as a function of the amplifier angle ϕ and stiffness factor κ_a for the cantilever with the stiffened inertial amplifier. The value of mass factor μ_a is considered 0.1 for this graph. For smaller amplifier angles $\phi \lessapprox 10^\circ$, the inertial amplification becomes prominent.

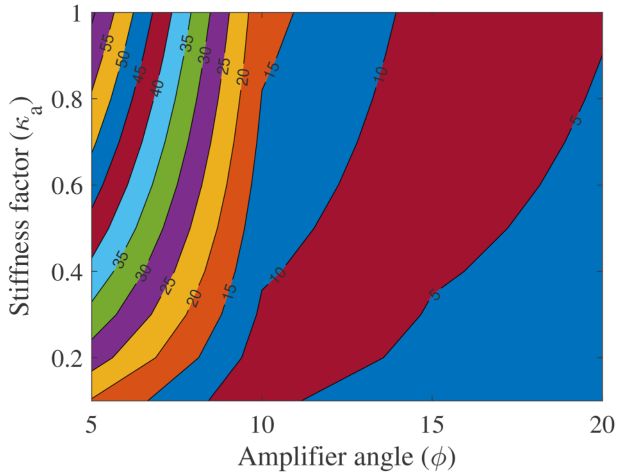

FIG. 6. The contour graph of the Q-factor amplification coefficient as a function of the amplifier angle ϕ and stiffness factor κ_a for the cantilever with the compound stiffened inertial amplifier. The value of mass factor μ_a is considered 0.1, and the secondary angle is considered $\theta = 70^\circ$ for this graph. For smaller amplifier angles $\phi \lessapprox 10^\circ$, the inertial amplification becomes prominent.

Another point to be noted is that the inertial amplifier effectively does not provide significant amplification when $\phi > 20^\circ$. Therefore, the amplifier angle should be chosen to be smaller than 20°. The amplification coefficient of the Q-factor is graphed as a function of the angle ϕ in Fig. 6. It has been noted that the Q-factor amplification increases when the amplifier angle ϕ approaches or exceeds $\phi \geq 5^\circ$. The obtained result demonstrates that the theoretical Q-factor amplification can exceed 60. The compound stiffened inertial amplifier has enhanced 2 the Q-factor of the cantilever beam compared to the stiffened inertial amplifier. The graph in Fig. 7 shows the amplification coefficient of the Q-factor as a function of the angle ϕ_1. It has been observed that the Q-factor amplification increases as the amplifier angle ϕ_1 approaches or exceeds $\phi_1 \geq 5^\circ$. The data obtained shows that the theoretical amplification of the Q-factor can surpass 3000. The nested stiffened inertial amplifier has a Q-factor that is twice and 100 as high as the compound stiffened inertial amplifier and stiffened inertial amplifier for the cantilever beam.

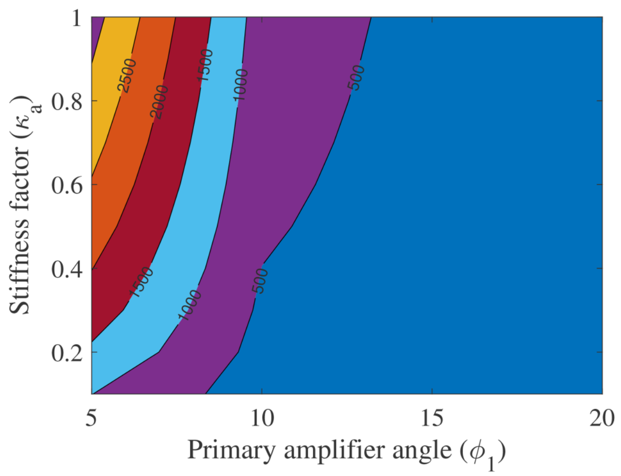

FIG. 7. The contour graph of Q-factor amplification coefficient as a function of the primary amplifier angle ϕ_1 and stiffness factor κ_a for the cantilever with the compound stiffened inertial amplifier. The value of mass factor μ_a is considered 0.1, and the secondary angle is considered $\phi_2 = 70^\circ$ for this graph. The tertiary angle is considered $\phi_3 = 15^\circ$. For smaller amplifier angles $\phi_1 \lessapprox 10^\circ$, the inertial amplification becomes prominent.

V. CONCLUSIONS

This paper presents and examines a new method for greatly improving the Q-factor of microcantilevers by employing stiffening inertial amplifiers. Our theoretical research shows that by using three different configurations, namely, ordinary stiffening amplifiers, compound amplifiers, and nested amplifiers, we can significantly enhance the sensitivity and performance of microcantilevers in sensing applications. The nested arrangement demonstrates remarkable potential, attaining Q-factor amplification that surpasses 3000 in optimal circumstances.

This work's main contribution is the utilization of inertial amplification principles in microcantilever technology. This approach provides a scalable and practical way to surpass the constraints of previous methods like material optimization and geometric modification. This novel methodology offers a means to significantly enhance the detection capabilities of microcantilevers, particularly in high-precision applications such as chemical, biological, and environmental sensing.

Subsequent efforts will prioritize the empirical verification of these theoretical models and the optimization of amplifier designs to improve their practical utility. Through the examination of how these designs can be included in microcantilever-based systems, we anticipate enhancing the Q-factor and expanding the range of applications that can take advantage of improved performance. This study contributes to the knowledge of improving the Q-factor in microcantilevers and creates possibilities for creating highly sensitive sensors in several areas of applied physics and engineering. For the future scope of the research, we aim to fabricate a microcantilever prototype, including inertial amplification mechanisms, using contemporary microfabrication methods for experimental validation.

ACKNOWLEDGMENTS

The authors would like to acknowledge the post-doctoral grant received from the University of Glasgow during this research work period.

AUTHOR DECLARATIONS

Conflict of Interest

The authors have no conflicts to disclose.

Author Contributions

Sondipon Adhikari: Conceptualization (equal); Data curation (equal); Formal analysis (equal); Investigation (equal); Methodology (equal); Project administration (equal); Resources (equal); Software (equal); Supervision (equal); Validation (equal); Visualization (equal); Writing – original draft (equal); Writing – review & editing (equal). **Sudip Chowdhury:** Conceptualization (equal); Data curation (equal); Formal analysis (equal); Funding acquisition (equal); Investigation (equal); Methodology (equal); Resources (equal); Software (equal); Validation (equal); Visualization (equal); Writing – original draft (equal); Writing – review & editing (equal).

DATA AVAILABILITY

All data, models, and code generated or used during the study are available within the article.

REFERENCES

[1] J. Leng, J. Peng, A. Jin, D. Cao, D. Liu, X. He, F. Lin, and F. Liu, "Investigation of terahertz high Q-factor of all-dielectric metamaterials," Opt. Laser Technol. **146**, 107570 (2022).
[2] Y. Tao, X. Li, T. Xu, H. Yu, P. Xu, B. Xiong, and C. Wei, "Resonant cantilever sensors operated in a high-Q in-plane mode for real-time bio/chemical detection in liquids," Sens. Actuators, B **157**, 606 (2011).
[3] S. Alaie, M. Hossein-Zadeh, M. G. Baboly, M. Zamani, and Z. C. Leseman, "Enhancing mechanical quality factors of micro-toroidal optomechanical resonators using phononic crystals," J. Microelectromech. Syst. **25**, 311 (2016).
[4] G. Anetsberger, R. Rivière, A. Schliesser, O. Arcizet, and T. J. Kippenberg, "Ultralow-dissipation optomechanical resonators on a chip," Nat. Photonics **2**, 627 (2008).
[5] L. Guo, M. Guo, H. Yang, J. Ma, and S. Chen, "Ultra-narrow-band filter based on high Q factor in metallic nanoslit arrays," Sensors **20**, 5205 (2020).
[6] S. Adhikari and A. Banerjee, "Enhanced low-frequency vibration energy harvesting with inertial amplifiers," J. Intell. Mater. Syst. Struct. **33**, 822 (2022).
[7] F. Rahman and M. S. Akanda, "Mechanical and dynamic characteristics of double and single beam cantilevers for MEMS manipulation," J. Mech. Sci. Technol. **36**, 4635 (2022).
[8] E. A. Corbin, A. YekrangSafakar, O. Adeniba, A. Gupta, K. Park, and R. Bashir, "Integrated cantilever-based biosensors for the detection of chemical and biological entities," in *Nanotechnology in Biology and Medicine* (CRC Press, 2017), pp. 469–530.
[9] R.-R. Xie, G.-Q. Li, F. Chen, and G.-L. Long, "Microresonators in lithium niobate thin films," Adv. Opt. Mater. **9**, 2100539 (2021).
[10] X. Zhang, J. Ding, X.-S. Zhu, and Y.-W. Shi, "Numerical simulation of optical fiber Tamm plasmon polariton sensor based on D-shaped hollow-core photonic crystal fiber coated with a gold film," IEEE Sens. J. **24**(5), 6207–6212 (2024).
[11] A. Alshammri, R. Alsaigh, K. E. Alzahrani, A. K. Assaifan, H. Albrithen, M. Braim, S. Pandiaraj, A. V. Juliet, G. Sanchana, F. H. Alkallas *et al.*, "Quality factor of a microchannel microresonator as a function of viscosity and its vibrational mode: An experimental and computational analysis," IEEE Sens. J. **23**, 104 (2022).
[12] V. Vassiliev and M. Sumetsky, "High Q-factor reconfigurable microresonators induced in side-coupled optical fibres," Light: Sci. Appl. **12**, 197 (2023).
[13] S. Mahashabde, E. Otto, D. Montemurro, S. de Graaf, S. Kubatkin, and A. Danilov, "Fast tunable high-Q-factor superconducting microwave resonators," Phys. Rev. Appl. **14**, 044040 (2020).
[14] J. Lu, T. Ikehara, T. Kobayashi, R. Maeda, and T. Mihara, "Quality factor of micro cantilevers transduced by piezoelectric lead zirconate titanate film," Microsyst. Technol. **13**, 1517 (2007).
[15] S. Banerji, P. Michalik, D. Fernández, J. Madrenas, A. Mola, and J. Montanyà, "CMOS-mems resonant pressure sensors: Optimization and validation through comparative analysis," Microsyst. Technol. **23**, 3909 (2017).
[16] C. C. Nguyen and W. L. Li, "Influences of temperature on the quality factors of micro-beam resonators in gas rarefaction," Sensors and Actuators A: Physical **261**, 151 (2017).
[17] J. Liu, T. B. Workie, T. Wu, Z. Wu, K. Gong, J. Bao, and K.-Y. Hashimoto, "Q-factor enhancement of thin-film piezoelectric-on-silicon MEMS resonator by phononic crystal-reflector composite structure," Micromachines **11**, 1130 (2020).
[18] G. Sun, L. Yuan, Y. Zhang, X. Zhang, and Y. Zhu, "Q-factor enhancement of fano resonance in all-dielectric metasurfaces by modulating meta-atom interactions," Sci. Rep. **7**, 8128 (2017).
[19] B. Xu, P. Zhang, J. Zhu, Z. Liu, A. Eichler, X.-Q. Zheng, J. Lee, A. Dash, S. More, S. Wu *et al.*, "Nanomechanical resonators: Toward atomic scale," ACS Nano **16**, 15545 (2022).
[20] M. Abtahi, G. Vossoughi, and A. Meghdari, "Full operational range dynamic modeling of microcantilever beams," J. Microelectromech. Syst. **22**, 1190 (2013).
[21] G. Sosale, K. Das, L. Fréchette, and S. Vengallatore, "Controlling damping and quality factors of silicon microcantilevers by selective metallization," J. Micromech. Microeng. **21**, 105010 (2011).
[22] M. Janneh, A. De Marcellis, E. Palange, A. Tenggara, and D. Byun, "Design of a metasurface-based dual-band terahertz perfect absorber with very high Q-factors for sensing applications," Opt. Commun. **416**, 152 (2018).
[23] H. Zhang, C. Liu, C. Xu, Z. Li, Y. Wang, and Y. Peng, "A dual-band terahertz metamaterial sensor with high Q-factor and sensitivity," Opt. Quantum Electron. **55**, 1126 (2023).
[24] J. Lu, T. Ikehara, Y. Zhang, T. Mihara, T. Itoh, and R. Maeda, "Characterization and improvement on quality factor of microcantilevers with self-actuation and self-sensing capability," Microelectron. Eng. **86**, 1208 (2009).
[25] W. J. Venstra, H. J. Westra, and H. S. van der Zant, "Q-factor control of a microcantilever by mechanical sideband excitation," Appl. Phys. Lett. **99**, 151904 (2011).
[26] H. Wen, *Toward Inertial-Navigation-on-Chip: The Physics and Performance Scaling of Multi-Degree-of-Freedom Resonant MEMS Gyroscopes* (Springer Nature, 2019).
[27] L. Sang, M. Liao, X. Yang, H. Sun, J. Zhang, M. Sumiya, and B. Shen, "Strain-enhanced high Q-factor GaN micro-electromechanical resonator," Sci. Technol. Adv. Mater. **21**, 515 (2020).
[28] A. R. Klempner, R. T. Marinis, P. Hefti, and R. J. Pryputniewicz, "Experimental determination of the Q-factors of microcantilevers coated with thin metal films," Strain **45**, 295 (2009).
[29] K. Y. Yasumura, T. D. Stowe, E. M. Chow, T. Pfafman, T. W. Kenny, B. C. Stipe, and D. Rugar, "Quality factors in micron-and submicron-thick cantilevers," J. Microelectromech. Syst. **9**, 117 (2000).
[30] M. W. Fairbairn, S. R. Moheimani, and A. J. Fleming, "*Q* control of an atomic force microscope microcantilever: A sensorless approach," J. Microelectromech. Syst. **20**, 1372 (2011).